Polymer 302 (2024) 127075

Contents lists available at ScienceDirect

Polymer

journal homepage: www.elsevier.com/locate/polymer

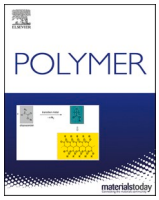

ABC block copolymer micelles driving the thermogelation: Scattering, imaging and spectroscopy

Anna P. Constantinou [a], Valeria Nele [a,b,c], James J. Doutch [d], Talia A. Shmool [e], Shaobai Wang [a], Qian Li [a], Jason P. Hallett [e], Cécile A. Dreiss [f], Molly M. Stevens [a,b,c], Theoni K. Georgiou [g,*]

[a] Department of Materials, Imperial College London, London, SW7 2AZ, UK
[b] Department of Bioengineering, Imperial College London, London, SW7 2AZ, UK
[c] Institute of Biomedical Engineering, Imperial College London, London, SW7 2AZ, UK
[d] ISIS Neutron and Muon Source, STFC, Rutherford Appleton Laboratory, Didcot, OX11 ODE, UK
[e] Department of Chemical Engineering, Imperial College London, London, SW7 2AZ, UK
[f] Institute of Pharmaceutical Science, King's College London, Franklin-Wilkins Building, 150 Stamford Street, London, SE1 9NH, UK
[g] Polymer Chemistry, Department of Materials, Imperial College London, Royal School of Mines, Exhibition Road, London, SW7 2AZ, UK

A B S T R A C T

Thermoresponsive polymers have attracted much scientific attention due to their capacity for temperature-driven hydrogel formation. For biomedical applications, such as drug delivery, this transition should be tuned below body temperature to facilitate controlled and targeted drug release. We have recently developed a thermoresponsive polymer that forms gel at low concentrations (2 w/w%) in aqueous media and offers a cost-effective alternative to thermoresponsive systems currently being applied in clinics. This polymer is an ABC triblock terpolymer, where A, B, and C correspond to oligo(ethylene glycol) methyl ether methacrylate with average M_n 300 g mol^{-1} (OEGMA300), *n*-butyl methacrylate (BuMA), and di(ethylene glycol) methyl ether methacrylate (DEGMA). To investigate the self-assembly and the gelation mechanism in diluted solutions, we used small-angle neutron scattering (SANS) on 1 w/w% (below the gelation concentration) and 5 w/w% solutions (above the gelation concentration). As a comparison, we also investigated the solutions of the most studied thermoresponsive polymer, namely, Pluronic F127, an ABA triblock bipolymer made of ethylene glycol (A) and propylene glycol (B) blocks. SANS revealed that the *in-house* synthesised polymer forms elliptical cylinders, whose length increases significantly with temperature. In contrast, Pluronic F127 solutions form core-shell spherical micelles, which slightly elongate with temperature. Transmission electron microscopy images support the SANS findings, with tubular/worm structures being present. Variable-temperature circular dichroism (CD) and proton nuclear magnetic resonance (^{1}H NMR) spectroscopy experiments reveal insights on the tacticity, structural changes, and molecular origin of the self-assembly.

1. Introduction

Thermoresponsive block copolymers are amphiphilic polymers which comprise at least a hydrophobic block and a hydrophilic and thermoresponsive block; the hydrophilicity of the latter changes with temperature. These polymers self-assemble into micelles and the thermal response is manifested by a cloud point in dilute conditions, while at higher concentrations, they form a 3-D network. Several underlying gelation mechanisms have been reported in the literature regarding this temperature-driven network formation, such as micellar packing, bridging of flower-like micelles, and micelle elongation [1].

Pluronics are commercially available thermoresponsive polymers with temperature-driven self-assembly, whose gelation is known to be attributed to micellar packing. More specifically, these polymers are ABA triblock bipolymers with A blocks being ethylene glycol (EG) and the central B block consisting of propylene glycol (PG). Below the critical micellisation temperature (CMT), PG units are hydrophilic, thus their aqueous solutions consist of unimers and aggregates. PG units gradually become hydrophobic with increasing temperature, thus these copolymers become amphiphilic and self-assemble into micelles at the CMT. When in concentrated solutions, polymer network formation occurs. The most widely studied Pluronic is F127 (average molar mass, MM, ≈12,600 g mol^{-1} and PG content 30 %), as it presents the lowest gelation concentration. Thus, it has been studied in several fields, such as biomedical engineering [2,3], drug delivery [4–6], 3-D printing [7–9], and formulation chemistry, primarily as a gelling agent [10,11]. Its self-assembly and gelation mechanisms have been extensively investigated, and small-angle neutron scattering (SANS) studies have revealed a temperature- and concentration-driven self-assembly into core-shell spherical micelles [12–15], whose packing into a

* Corresponding author.
E-mail address: t.georgiou@imperial.ac.uk (T.K. Georgiou).

https://doi.org/10.1016/j.polymer.2024.127075
Received 7 February 2024; Received in revised form 13 April 2024; Accepted 15 April 2024
Available online 18 April 2024

body-centred-cubic (BCC) structure is responsible for gelation [16].

The gelation mechanism of a triblock copolymer consisting of an EG-based hydrophilic central block, and two hydrophobic outer blocks consisting of butylene glycol was also studied through scattering techniques by Castelletto et al. [17] This type of amphiphilic copolymer is expected to form flower-like micelles, whereby polymer chains loop back to insert their hydrophobic end-blocks within the core of the micelles (forming the petals of the flower) or act as bridges between adjacent micelles. SANS studies on the diluted solutions revealed that the polymer chains act as bridges between the micelles, which increase in number as a function of the polymer concentration, thus leading to stronger gels (i.e., gels with a higher storage modulus, G′, as measured by oscillatory shear rheology). Small-angle X-ray scattering (SAXS) showed that the organisation of the micelles in the gel state is characterised by a BCC structure [17].

Thermoresponsive gelation can also be achieved by the formation of wormlike micelles with diblock copolymers, as has been reported by Armes' group [18–20]. In their first study, diblock copolymers comprising of poly(2-hydroxypropyl methacrylate) (PHPMA) and poly (glycerol monomethacrylate) were investigated [19]. Visual tests and rheological measurements revealed a transition from solution (at 4 °C) to gel (at 21 °C) while transmission electron microscopy (TEM) and SAXS revealed that this behaviour could be explained by a shape transition from spherical micelles (at 4 °C) to wormlike micelles (at 21 °C) [19]. Recently, similar findings were reported for a diblock copolymer consisting of poly(2-(methacryloyloxy)ethyl phosphorylcholine and PHPMA [20]. In another study by the same group, a novel diblock copolymer, namely, poly(*N*,*N*-dimethacrylamide)-poly(4-hydroxybutyl acrylate-*stat*-diacetone acrylamide), showed sol-gel-sol-gel transition upon heating, as confirmed visually and by rheology [18]. Interestingly, this unique transition was caused by a change in the self-assembly from spheres (solution at 1 °C) to worm-like structures (gel at 25 °C), to vesicles (solution at 50 °C), to lamellae (gel at 70 °C), as revealed by TEM and SAXS [18].

Most of the published studies on this topic focus on diblock and triblock bipolymers, due to their abundance in the literature, attributed primarily to their easier synthesis. To the best of our knowledge, only a limited number of studies has investigated the gelation mechanism of ABC triblock terpolymers. Lodge's group has also reported the investigation of ABC triblock terpolymers, poly(ethylene-*alt*-propylene)-*b*-polyEG-*b*-poly(*N*-isopropylacrylamide) (PON) [21,22] and poly(1, 2-butadiene)-*b*-polyEG-*b*-poly(perfluoropropylene oxide) [23] by means of SAXS and SANS. In addition, double-responsive, i.e., pH- and thermoresponsive, triblock terpolymers were investigated by SANS; these triblock terpolymers are poly(2-vinylpyridine)-*b*-polyEG-*b*-poly(glycidyl methyl ether-*co*-ethyl glycidyl ether) [24,25] and polystyrene-*b*-poly (2-vinylpyridine)-*b*-polyEG [26].

Our group has previously reported a new family of thermoresponsive ABC triblock terpolymers of constant MM and varying compositions, where A, B and C consist of oligo(ethylene glycol) methyl methacrylate with number-average MM (M_n) 300 g mol^{-1} (OEGMA300), *n*-butyl methacrylate (BuMA) and di(ethylene glycol) methyl ether methacrylate (DEGMA), respectively [27]. A member of this family, namely OEGMA300$_{16}$-*b*-BuMA$_{28}$-*b*-DEGMA$_{15}$, Fig. 1, presents interesting gelation properties, with a critical gelation concentration as low as 2 w/w%, as revealed by visual tests and rheology. This observation in combination with the limited literature investigating the gelation mechanism of ABC triblock terpolymers prompt an in-depth investigation of its self-assembly and gelation mechanism. In the current study, we investigate its aqueous solutions at 1 w/w% and 5 w/w% over a range of temperatures by SANS and compare with the corresponding solutions of Pluronic F127. In addition to investigating the self-assembly of these polymers at the nanoscale, we visualise the self-assembled structures by both cryogenic and conventional transmission electron microscopy (cryoTEM and TEM, respectively). Finally, we also monitor temperature-driven structural changes by circular dichroism (CD) and nuclear magnetic resonance (NMR) spectroscopy.

2. Experimental

2.1. Materials

Pluronic F127, average MM 12600 g mol^{-1} and ≈70 % EG, phosphate buffered saline (PBS) tablets, and deuterium oxide (D_2O) were purchased from Sigma Aldrich Ltd., UK. The ABC triblock terpolymer was synthesised via group transfer polymerisation (GTP), and the synthesis has been previously reported [27]. Cuvettes for dynamic light scattering (DLS) experiments were purchased from VWR International.

2.2. Methods

2.2.1. Dynamic light scattering (DLS)

The solutions of the polymers at 1 w/w% in D_2O/PBS (same solvent as in SANS) were measured by dynamic light scattering (DLS) with temperature ramps using a Zetasizer Nano ZSP (Malvern Instruments Ltd), and the data analysis was performed using a Zetasizer software (version 7.11) from Malvern Panalytical. The scattered light was collected at a backscatter angle of 173°, and the sample was analysed three times at each temperature step. One should bear in mind that DLS technique assumes the formation of spheres.

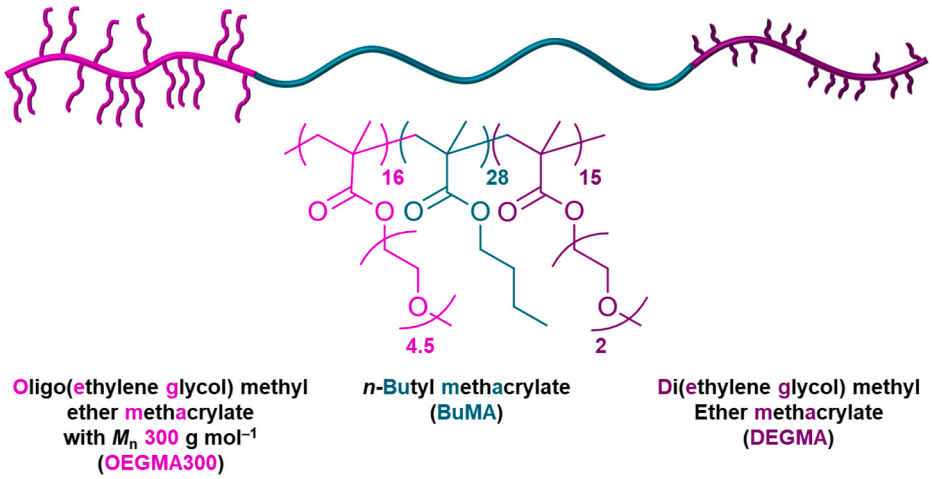

Fig. 1. Schematic representation and chemical structure of the ABC triblock terpolymer.

2.2.2. Small-angle neutron scattering (SANS)

Temperature ramp measurements were performed on solutions of the polymers (1 and 5 w/w%) in D_2O/PBS and monitored by SANS. The experiments were performed at the ISIS pulsed neutron source at the Rutherford Appleton Laboratory (Didcot, UK), using a time-of-flight SANS instrument ZOOM, and a source to sample and sample to detector distance of 4 m, and wavelength range 1.5–16.5 Å. The instrument was equipped with an Anton Paar rheometer (Physica MCR501), loaded with a special Searle-Couette (rotating stator) measuring geometry in Grade-V Titanium. The strain was kept constant at 1 %, and the angular frequency at 1 rad s^{-1}. As the mechanical perturbations applied were small (within the linear viscoelastic area), the conformation of the polymers was not disrupted, thus the analysis and discussion are focused on the structure (rather than any effect of shear). During this experiment, the beam travelled through the centre of the geometry, and the temperature was kept constant while collecting the SANS data, with each step lasting 6 min and 7 s. Data reduction was performed using MantidPlot [28].

2.2.3. Modelling of SANS data

The results were fitted using SasView software (versions 5.0 for OEGMA300$_{16}$-*b*-BuMA$_{28}$-*b*-DEGMA$_{15}$ and 4.2.2 for Pluronic F127) [28,29]. Scattering curves from OEGMA300$_{16}$-*b*-BuMA$_{28}$-*b*-DEGMA$_{15}$ micelles were best fitted to an elliptical cylinder model (minor radius, major radius and length of the cylinder), as ellipsoid model showed poorer quality fits. The scattering length density (SLD) value of the solvent (D_2O/PBS) was fixed at 6.36 × 10^{-6} $Å^{-2}$ and the SLD of the polymer at 0.64 × 10^{-6} $Å^{-2}$. The SANS data for the 1 % solution were not fitted above 38 °C, as phase separation occurs. At 5 %, the samples form a gel at higher temperatures, which was fitted using a BroadPeak model (peak position in q, $Å^{-1}$); the gel then destabilises via syneresis and precipitation at the highest temperatures. Scattering curves from Pluronic F127 were fitted to a core-shell sphere model with a hard-sphere structure factor. To take into consideration the contribution from the poly(ethylene glycol) PEG shell, as well as unimers in solution – visible in the high-q region –, a Gaussian coil with $R_g = 7$ Å was added to the modelling, similarly to previous studies [15]. In order to reduce the number of fitting parameters, the SLD values were kept constant at 6.00 × 10^{-6} $Å^{-2}$ for the shell and at 6.36 × 10^{-6} $Å^{-2}$ for the solvent (D_2O/PBS). The SLD of the core was kept fixed at 1.5 × 10^{-6} $Å^{-2}$ for the 1 w/w% solution, indicating a slightly hydrated core, as previously observed [14], while the SLD of the core was kept fixed at 0.4 × 10^{-6} $Å^{-2}$ for the 5 w/w% solution, indicating a very dehydrated core, as in previous studies on similar systems [15,30–32]. The polydispersity of the core size and the shell thickness of the micelles were also fixed, to 0.15 and 0.2, respectively, as in previous work [14].

2.2.4. Transmission electron microscopy (TEM)

The self-assembled structures of both copolymers at 1 w/w% and 5 w/w% in deionised water were visualised via TEM. For sample preparation, 10 μL of the aqueous polymer solution was pipetted onto an S160 carbon film on 200 mesh grid copper (Agar Scientific Ltd, UK). Once 60 s have passed, the excess of sample was removed using a filter paper, and subsequently the sample was washed by pipetting 30 μL of DI water. For achieving contrast on the TEM, the samples were negatively stained by using 2 w/v% uranyl acetate. The staining was performed by pipetting 30 μL of stain solution, while holding the TEM grids at an angle of 45°, and the sample was left to air dry. The TEM images were recorded using a JEOL STEM 2100Plus transmission electron microscope, operated at 80 kV to enhance contrast for bright field TEM, and by using an objective aperture of 70 μm.

2.2.5. Cryogenic Transmission Electron Microscopy (Cryo-TEM)

Cryo-TEM was performed on the samples of OEGMA300$_{16}$-*b*-BuMA$_{28}$-*b*-DEGMA$_{15}$ solution at 5 w/w% and 10 w/w% in PBS at room temperature (liquid state) and 37 °C (gel state). For visualising the self-assembly at room temperature, 5 μL of sample was applied to a glow-discharged Lacey carbon grid (EM Resolutions, UK) inside the chamber of a Leica GP2 plunge-freezing device held at 20 °C. Excess sample was blotted off in two 5s blotting steps before plunging in liquefied propane/ethane mixture. Samples were imaged using a Gatan 626 cryo-holder on a JEOL 2200FS TEM with a Gatan K2 direct electron detector. To image the sample at 37 °C, while it is at the gel state, the sample was manually blotted while held outside the chamber, then incubated inside the chamber at 37 °C for 200 s, before plunging into the propane/ethane mixture as for the room temperature samples.

2.2.6. Circular dichroism (CD) spectroscopy

Temperature variable CD experiments were performed on a Chirascan CD spectrometer (Applied Photophysics Ltd, Leatherhead, Surrey, UK) with a Quantum Northwest Peltier temperature controller (Quantum Northwest Inc., Liberty Lake, Washington, USA), as previously described [33]. Briefly, samples were placed in a quartz cuvette (Starna Scientific Ltd, Ilford, UK) and measured with a 1 °C min^{-1} heating rate between 25 °C and 45 °C with a 0.2 °C tolerance. Spectroscopic data was collected between 260 and 190 nm. For each sample, the phosphate buffered saline solvent was measured in triplicate at 25 °C, averaged and subtracted from the temperature variable CD data of each sample. The Origin software (OriginLab Corporation, Northampton, Massachusetts, USA) was used to analyse the data. The data was zero and smoothed using Savitzky–Golay method with 7 points and polynomial order 5 and the mean residual ellipticity (MRE) was calculated by accurately accounting for polymer mean residual weight and concentration.

2.2.7. Proton nuclear magnetic resonance (^{1}H NMR) spectroscopy

^{1}H NMR spectroscopy was performed using a JEOL400 NMR Spectrometer. Both OEGMA300$_{16}$-*b*-BuMA$_{28}$-*b*-DEGMA$_{15}$ and Pluronic F127 were analysed in $CDCl_3$ at a concentration of 10 mg mL^{-1} (1 w/v%). The copolymers were also dissolved in D_2O at 10 w/w% and were analysed via ^{1}H NMR at different temperatures, specifically, 25 °C, 31 °C, and 37 °C (32 scans).

3. Results and discussion

3.1. Micellar structure of OEGMA300$_{16}$-b-BuMA$_{28}$-b-DEGMA$_{15}$

OEGMA300$_{16}$-*b*-BuMA$_{28}$-*b*-DEGMA$_{15}$ at 1 w/w% in PBS displays a thermal response reflected by a cloud point (38 °C) and precipitation (39 °C) [27]. This polymer presents a gelation concentration as low as 2 w/w% in PBS, with gelation temperature at 39 °C [27], and therefore understanding its self-assembly in diluted solutions is of major interest. Thus, SANS was used to investigate the effect of temperature on its self-assembly behaviour at 1 w/w%, which is below its gelation concentration, Fig. 2 a) and Table 1. To achieve a good neutron contrast, the experiments were performed in D_2O/PBS, in which the cloud point and precipitation were visually detected at 37 °C and 38 °C, respectively, equal to PBS only, within the error of the technique (±2 °C).

To preliminary assess the size evolution prior to the SANS measurements, we performed DLS measurements at different temperatures, Fig. S1. We observed a monomodal distribution with the average size of the aggregates which remained unchanged at approximately 35 nm up to 31 °C. Above 34 °C, the size increased drastically, reflecting aggregation into larger clusters, with sizes of the order of 100s of nm. This behaviour is indicative of a sharp transition in self-assembly structures just below physiological temperature. While DLS is useful to detect changes due to temperature, specific sizes are not discussed further, as the technique assumes a spherical shape from the scattering objects, which – as we show later from the SANS analysis – is incorrect.

SANS was used to provide an insight into the morphology of the aggregates. The scattering signals from the micelles of OEGMA300$_{16}$-*b*-BuMA$_{28}$-*b*-DEGMA$_{15}$ were best fitted to an elliptical cylinder model, i.e., a cylinder with an elliptical cross-section, as simpler models, such as

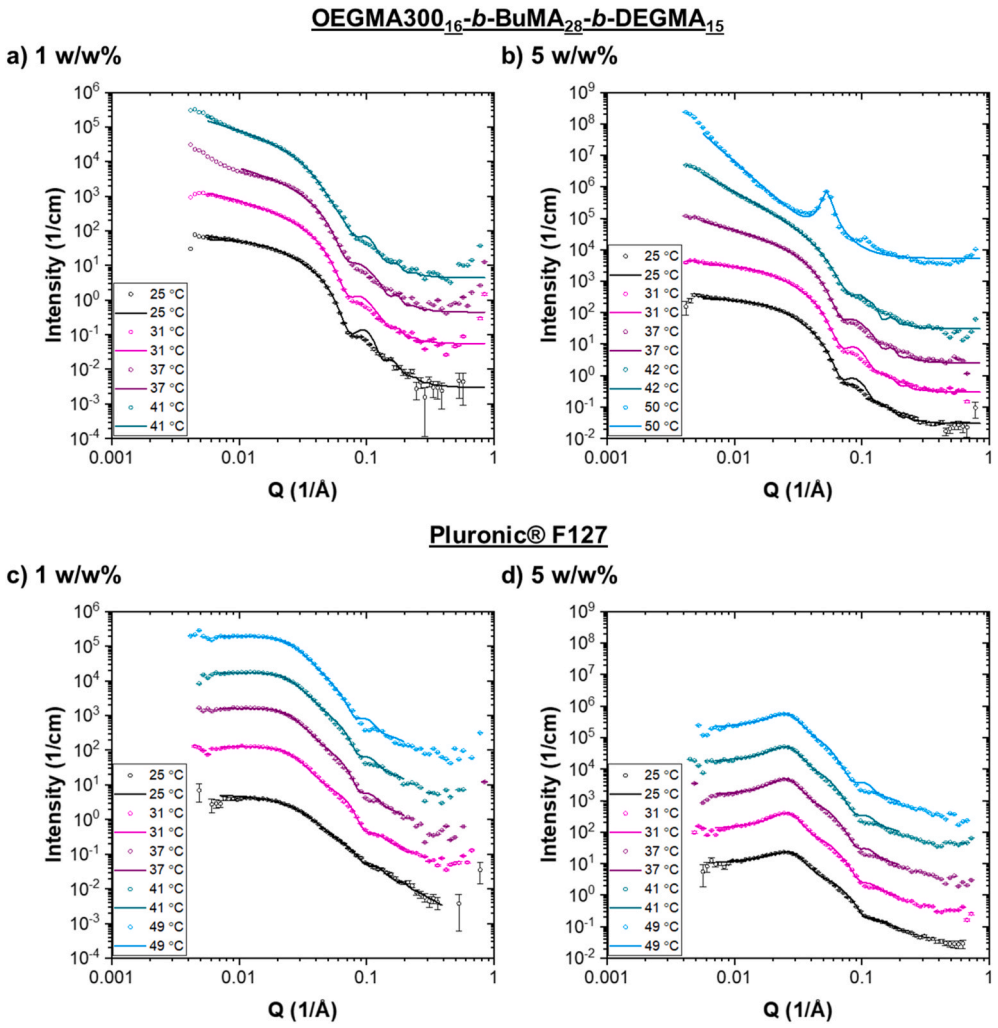

Fig. 2. Top – Small-angle neutron scattering curves from OEGMA300$_{16}$-*b*-BuMA$_{28}$-*b*-DEGMA$_{15}$ at different temperatures in D_2O/PBS at a) 1 w/w% and b) 5 w/w%. and c) Bottom – Small-angle neutron scattering curves from Pluronic F127 at different temperatures in D_2O/PBS of at c) 1 w/w% and d) 5 w/w%.

Table 1
Structural Parameters obtained by SANS analysis on solutions of OEGMA300$_{16}$-*b*-BuMA$_{28}$-*b*-DEGMA$_{15}$ at 1 w/w% in D_2O/PBS.

Temperature (°C)	Minor Radius (Å) ± 5 %	Major Radius (Å) ± 5 %	Length (Å) ± 5 %
23	48	59	243
25	48	60	235
27	48	61	240
29	47	65	420
31	46	66	600
33	46	67	730
34	47	68	720
35	47	69	660
36	44	65	590
37	47	69	506
38	46	68	526
39	47	70	547
40	49	77	562
41	47	80	1000

[a] SANS data were fitted to an elliptical cylinder model, i.e., a cylinder with an elliptical cross-section.

ellipsoid, did not provide the best fits. Representative SANS profiles are presented in Fig. 2 a), and the complete set of data is shown in Figs. S2–S4. The best-fit minor radius decreased slightly from 48 Å to 44 Å as the temperature was increased from 23 °C to 36 °C (Figure S4 a) and Table 1), while the best-fit major radius increased from 59 Å to 65 Å as the temperature was increased from 23 °C to 36 °C, Table 1. Interestingly, the best-fit length of the elliptical cylinder was 235 Å at room temperature, and it gradually increased, reaching values of the order of 500–700 Å (Figure S4 b). Beyond the onset of precipitation (visually detected at 38 °C), a slight upturn at low q could be an indication of a sharp interface, suggesting the presence of very large aggregates not measured by SANS, while the values obtained for the cylinders is indicative only (due to the likely presence of other structures). This elongation explains the drastic size increase observed in DLS measurements.

To investigate the self-assembly of OEGMA300$_{16}$-*b*-BuMA$_{28}$-*b*-DEGMA$_{15}$ above its critical gelation concentration (2 w/w%), its solution at 5 w/w% in D_2O/PBS was investigated by SANS over a range of temperatures. This sample visually forms a gel at 35 °C, which destabilises via gel syneresis at 46 °C, with the onset of precipitation taking place at 47 °C. The resulting scattering patterns were best fitted using an elliptical cylinder model up to 44 °C, Table 2, and Fig. 2 b), S5 and S6, while the data at higher temperatures, i.e., at temperatures at which the gel visually destabilises, were fitted with a Broadpeak model, Table 3, and Fig. S7.

The scattering patterns of OEGMA300$_{16}$-*b*-BuMA$_{28}$-*b*-DEGMA$_{15}$ solution at 5 w/w% and the effect of temperature are similar to the ones obtained at 1 w/w%, Fig. 2 b). Specifically, the scattering patterns show an increase in intensity in the low *q* region, with temperature increasing

Table 2
Structural Parameters obtained by SANS analysis on solutions of OEGMA300$_{16}$-*b*-BuMA$_{28}$-*b*-DEGMA$_{15}$ at 5 w/w% in D_2O/PBS up to 36 °C. *Note: the sample gels visually at 35 °C, and it remains stable up to 45 °C, above which, gel syneresis and precipitation are observed.*

Temperature (°C)	Minor Radius (Å) ± 5 %	Major Radius (Å) ± 5 %	Length (Å) ± 5 %
23	49	66	210
25	50	66	207
27	50	66	213
29	50	66	218
31	50	66	250
32	50	67	337
33	48	67	750
35	48	68	1050
36	48	69	2200
37	47	69	10000
38	47	72	10000
40	46	82	10000
42	45	394	10000
44	43	258	10000

[a]SANS data was fitted to an elliptical cylinder model, i.e., a cylinder with an elliptical crossection.

Table 3
Structural parameters obtained by SANS analysis on gels of OEGMA300$_{16}$-*b*-BuMA$_{28}$-*b*-DEGMA$_{15}$ at 5 w/w% in D_2O/PBS from 46 °C to 52 °C. *Note: the sample presents gel syneresis, followed by precipitation, at this temperature range.*

Temperature (°C)	Peak Position (Å^{-1})
46	0.046
48	0.050
50	0.053
52	0.055

[a]SANS data was fitted to a BroadPeak model [29].

from 31 °C to 42 °C. Upon heating to 46 °C, a peak appears at $q \approx 0.05$ Å^{-1}, whose position changes with temperature. These are discussed below in more detail.

From the values returned by the fits, the best fit to the minor radius of the elliptical cross-section of the cylinder remains relatively stable at around 48 Å to 50 Å up to 36 °C, Table 2 and Figure S8 a). The values as well as the trend are similar to the ones obtained with the 1 w/w% solution. In addition, the length of the elliptical cylinder drastically increases from 210 Å (at 23 °C) to 750 Å (at 33 °C), which is below the visual gelation temperature of 35 °C, Figure S8 b). At the onset of the gelation, the elliptical cylinder model is unable to describe the data at low-q, which likely reflects further drastic elongation of the micelles (sizes beyond the size measurable by SANS), or the appearance of larger clusters in solution, Table 2.

As the temperature increases further, the gel destabilises by means of gel syneresis, i.e., shrinking of the gel due to internal forces [34,35], which is visually observed at 46 °C as a slight exclusion of solvent. The sample progressively excludes more solvent as the temperature increases further, and precipitation is observed at 47 °C. Starting from 46 °C, a peak is noticeable in the scattering data at $q \approx 0.05$ Å^{-1}. Therefore, the data were best fitted using the "Broadpeak model" [29], which suggests the presence of scattering inhomogeneities, such as lamellar, cylindrical, or bicontinuous structures [36]. The peak position shifts from 0.046 Å^{-1} to 0.055 Å^{-1} with temperature, indicating that the distance between the scattering inhomogeneities decreases from 136 Å to 113 Å. This can be explained as the polymer network progressively excludes more solvent, thus the aggregates come closer to each other, until eventually complete phase separation is achieved.

3.2. Micellar structure of Pluronic F127

As OEGMA300$_{16}$-*b*-BuMA$_{28}$-*b*-DEGMA$_{15}$ outperforms Pluronic F127 in terms of low gelation concentration [27], the most studied thermoresponsive polymer in the scientific community [37], we investigated the self-assembly of Pluronic F127 at 1 w/w% in D_2O/PBS by SANS for comparison.

DLS temperature ramp measurements were performed to first assess the size evolution, similarly to OEGMA300$_{16}$-*b*-BuMA$_{28}$-*b*-DEGMA$_{15}$ solution. At temperatures close to its critical micellisation temperature (CMT), determined at 24 °C for 1 % solution in D_2O [13], the coexistence of unimers and micelles is observed up to 25 °C, Fig. S9. In addition to the unimers and micelles, very large aggregates with hydrodynamic diameter larger than 200 nm were also detected at the lower temperatures. This feature is often observed in Pluronic and Tetronic solutions, and it is attributed to clusters of hydrophobic impurities in the form of mono- or diblock copolymers, which then become solubilised in the hydrophobic core of the micelles at higher temperatures [32,38,39]. Upon completion of the micellisation, monomodal distribution with sizes corresponding to the micelles was observed up to 51 °C. This shows the temperature-driven self-assembly of Pluronic F127, caused by the thermoresponse of the poly(propylene glycol) (PPG) middle block. This is in contrast with the self-assembly of OEGMA300$_{16}$-*b*-BuMA$_{28}$-*b*-DEGMA$_{15}$, which consists of a permanently hydrophobic middle block, namely BuMA, thus thermodynamically favouring its self-assembly to avoid interactions with water.

The scattering patterns of Pluronic F127 at 1 w/w% show an increase in intensity upon heating, Fig. 2 c), S10, and S11. In addition, while the signal at high q at 23 °C and 25 °C, which is around the CMT, corresponds to the one expected for polymer chains, starting from 27 °C, the signal becomes more characteristic of structured, spherical objects, here micelles. These general observations agree with the results obtained by DLS measurements.

The SANS signals of Pluronic F127 at 23 °C and 25 °C were fitted with a combination of core-shell sphere model and the Guinier-Debye model for Gaussian coils, which describes solvated polymer coils in a *theta* solvent. At higher temperatures, a core-shell sphere model combined with a hard-sphere structure factor was used instead, indicating a significant change in the morphology of the scattering objects, i.e., a transition from random coils to micelles. The SLD of the solvent was fixed at 6.36×10^{-6} Å^{-2}, while the SLD of the shell was fixed at 6×10^{-6} Å^{-2}, indicating a highly solvated corona, similarly to previous studies on this polymer [15]. The SLD of the core was initially let to vary, resulting in values close to 1.5×10^{-6} Å^{-2}, thus it was fixed to this value to minimise the number of parameters to fit. This value is higher than 0.4×10^{-6} Å^{-2}, the SLD value corresponding to the PPG block [14,15], indicating that the core is hydrated at ca. 18 %. At 23 °C, data analysis returned a radius of gyration of the unimers at 58 Å, lying within the range reported previously [13], and a core radius of 48 Å and shell thickness of 61 Å for the micelles, Table 4. Similar results were obtained at 25 °C. At higher temperatures, at which the complete transition from unimers to micelles is observed, data analysis returned a core radius of 43 Å and a shell thickness of 67 Å at 29 °C, Table 4, and Fig. S12. These values are in a good agreement with values reported at 29 °C for Pluronic F127 at 1 % in D_2O, with a 42 Å core radius and 61 Å shell thickness [13]. When compared to OEGMA300$_{16}$-*b*-BuMA$_{28}$-*b*-DEGMA$_{15}$ under the same conditions, the major radius of OEGMA300$_{16}$-*b*-BuMA$_{28}$-*b*-DEGMA$_{15}$ is slightly smaller than the total radius of the sphere adopted by Pluronic F127 (65 Å versus 110 Å). However, OEGMA300$_{16}$-*b*-BuMA$_{28}$-*b*-DEGMA$_{15}$ is considerably more elongated, as the best-fit length of the elliptical cylinder is 420 Å. As temperature increases from 31 °C to 37 °C, the core radius increases slightly from 44 Å to 48 Å, Table 4 and Fig. S12, in agreement with the observations of Grillo et al. [13].

As a comparison with OEGMA300$_{16}$-*b*-BuMA$_{28}$-*b*-DEGMA$_{15}$, the self-assembly of Pluronic F127 at 5 w/w% over a range of temperatures was

Table 4
Structural Parameters obtained by DLS and SANS analysis on solutions of Pluronic F127 at 1 w/w% in D_2O/PBS.

Temperature (°C)	Core Radius (Å) ± 5 %	Shell Thickness (Å) ± 5 %	Total Radius (nm)[a] ± 5 %
23	48	61	10.9
25	47	61	10.8
27	39	66	10.5
29	43	67	11.0
31	44	70	11.4
33	46	69	11.5
35	47	70	11.7
37	48	70	11.8
39	49	68	11.7
41	49	70	11.9
43	50	68	11.8
45	50	69	11.9
47	51	68	11.9
49	53	65	11.8
51	53	65	11.8

Note: SANS data at 23 °C and 25 °C were fitted using a combination of a core-shell sphere model and mono-gauss coils, while at higher temperatures, the data were fitted to core-shell model with a hard-sphere structure factor; a Gaussian coil ($R_g = 7$ Å) was used to fit the high-q region. For more information, please refer to the Experimental Section.

[a] The total radius (nm) has been calculated as the sum of the core radius and shell thickness; the values of the latter have been obtained through the fits.

also investigated via SANS (Fig. 2d)–Table 5, and Figs. S13–S14) using an analysis similar to previous studies [12,14,15]. For the analysis, the SLD of the shell was fixed at 6×10^{-6} Å^{-2}, in analogy to the analysis on 1 w/w% solution case and previous studies [15]. The SLD of the core could be fixed at 0.4×10^{-6} Å^{-2}, suggesting no solvent penetration, as previously observed in poloxamine micelles [14,15,30–32]. Fixing these parameters leads to core radius values increasing from 39 Å to 51 Å with a temperature increase from 23 °C to 51 °C, while the shell thickness varies from 59 Å to 66 Å, Table 5 and Fig. S15. These values are in good agreement with previously reported values on the same system [14,15].

3.3. Imaging of the micellar and gel structure

The solutions of both OEGMA300$_{16}$-*b*-BuMA$_{28}$-*b*-DEGMA$_{15}$ and Pluronic F127 at 1 w/w% and 5 w/w% at room temperature were imaged via TEM, Fig. 3. Near-spherical structures were captured for both polymers at 1 w/w% in deionised water, with the micelles of OEGMA300$_{16}$-*b*-BuMA$_{28}$-*b*-DEGMA$_{15}$ being slightly larger than those of Pluronic F127. More specifically, clear spherical structures of size around 15–25 nm in diameter are observed for OEGMA300$_{16}$-*b*-BuMA$_{28}$-*b*-DEGMA$_{15}$. These values agree with the ones resulted by DLS and SANS under the same conditions, which revealed hydrodynamic diameters of 32.7 nm (by intensity) and 15.7 nm (by number), and best-fit length of the elliptical cylinder of 23.5 nm. On the other hand, smaller micelles of around 10–14 nm in diameter are adopted by Pluronic F127, whose properties remain unchanged with increasing the concentration from 1 w/w% to 5 w/w%. These are slightly smaller than the ones detected by DLS and SANS (24.4 and 22 nm, respectively). Any minor differences could be attributed to TEM being performed in the dry state, while solvated self-assembled structures are analysed by DLS and SANS, an observation previously reported [40,41]. Interestingly, in OEGMA300$_{16}$-*b*-BuMA$_{28}$-*b*-DEGMA$_{15}$ solutions at 5 w/w%, co-existence of spherical structures with tubular/worm micelles is observed, with the diameter of both being in the same range as at 1 w/w%. This observation agrees with the cylindrical structures obtained by SANS analysis, as previously discussed.

To gain further insights on the self-assembly behaviour and gel formation of OEGMA300$_{16}$-*b*-BuMA$_{28}$-*b*-DEGMA$_{15}$ at 5 and 10 w/w% in PBS, we visualised the samples at 20 °C (free-flowing solution) and 37 °C (free-standing gel) by cryo-TEM, Fig. 4. Co-existence of spherical and tubular structures is observed, with the sizes being similar to the ones detected by TEM at 1 and 5 w/w% in deionised water (see Fig. 3). Localised mesh/tube structures are detected for the 5 w/w% sample at 37 °C, while a network formed by individual worm-like micelles is visualised at 10 w/w%, presumably due to the higher concentration.

Table 5
Structural Parameters obtained by DLS and SANS analysis on solutions of Pluronic F127 at 5 w/w% in D_2O/PBS.

Temperature (°C)	Core Radius (Å)[a] ± 5 %	Shell Thickness (Å)[a] ± 5 %	Total Radius (nm)[b] ± 5 %
23	39	61	10.0
25	40	64	10.4
27	42	65	10.7
29	43	66	10.9
31	45	66	11.1
33	46	66	11.2
35	46	66	11.2
37	47	65	11.2
39	48	64	11.2
41	48	63	11.1
43	49	63	11.2
45	49	62	11.1
47	50	60	11.0
49	50	61	11.1
51	51	59	11.0

[a] SANS data was fitted to core-shell model with a hard-sphere structure factor; a Gaussian coil ($R_g = 7$ Å) was used to fit the high-q region. For more information, please refer to the Experimental Section.

[b] The total radius (nm) has been calculated as the sum of the core radius and shell thickness; the values of the latter have been obtained through the fits.

3.4. Structural changes of triblock copolymers

The aqueous solutions of both OEGMA300$_{16}$-*b*-BuMA$_{28}$-*b*-DEGMA$_{15}$ and Pluronic F127 were tested at 1 and 5 w/w% in PBS by performing variable temperature circular dichroism (CD) spectroscopy experiments. The CD spectra of both polymers showed a minimum between approximately 210-220 nm, Fig. 5. Notably, the spectra of the OEGMA300$_{16}$-*b*-BuMA$_{28}$-*b*-DEGMA$_{15}$ samples presented deeper initial minima (Fig. 5 a) and 5b)) compared to the Pluronic F127 samples (Fig. 5d) and 5e)). We suggest that this is due to the lower number of asymmetric centres present in Pluronic F127 compared to OEGMA300$_{16}$-*b*-BuMA$_{28}$-*b*-DEGMA$_{15}$ [42], [[,43] as previously observed in poly(*N*-isopropylacrylamide-*co*-*N*-methacryloyl-*L*-leucine) copolymers [44]. More specifically, each methacrylate unit in OEGMA300$_{16}$-*b*-BuMA$_{28}$-*b*-DEGMA$_{15}$ contains a chiral carbon on the backbone, while Pluronic F127 contains an asymmetric carbon only in the PPG block.

Regarding OEGMA300$_{16}$-*b*-BuMA$_{28}$-*b*-DEGMA$_{15}$, we attribute the minimum of each sample to the n−π* and π−π* of the carbonyl group [45–47] on the methacrylate side chain and asymmetric carbon on the methacrylate backbone. The observation of the negative bands in this wavelength range, assigned to the n−π* and π−π* transitions has previously been reported in several polymeric systems, such as poly(*N*-isopropylacrylamide)-*b*-poly(*L*-glutamic acid) [48], and poly(*N*-isopropylacrylamide)-*b*-poly(glycidyl methacrylate-*g*-*L*-glutamic acid) [49]. Minimal changes are observed upon heating the 1 w/w% sample, consistent with the sample visually remaining in a runny solution state up to 39 °C, where the onset of precipitation is observed. As the temperature is raised further, a slight shift to higher wavelengths is observed. Interestingly, for the solution at 5 w/w%, we observe a shift in the minimun to higher wavelengths, and greatest change in intensity of the negative peak upon heating. As depicted in Fig. 5c), where the MRE (MRE$_{min}$) values are plotted as a function of temperature, a plateau is observed at low temperatures, likely corresponding to the runny solution state of the sample. An abrupt increase in the MRE$_{min}$ values is observed upon heating from 35 to 40 °C, where a second plateau is observed up to 45 °C. This is consistent with the visual formation of a gel

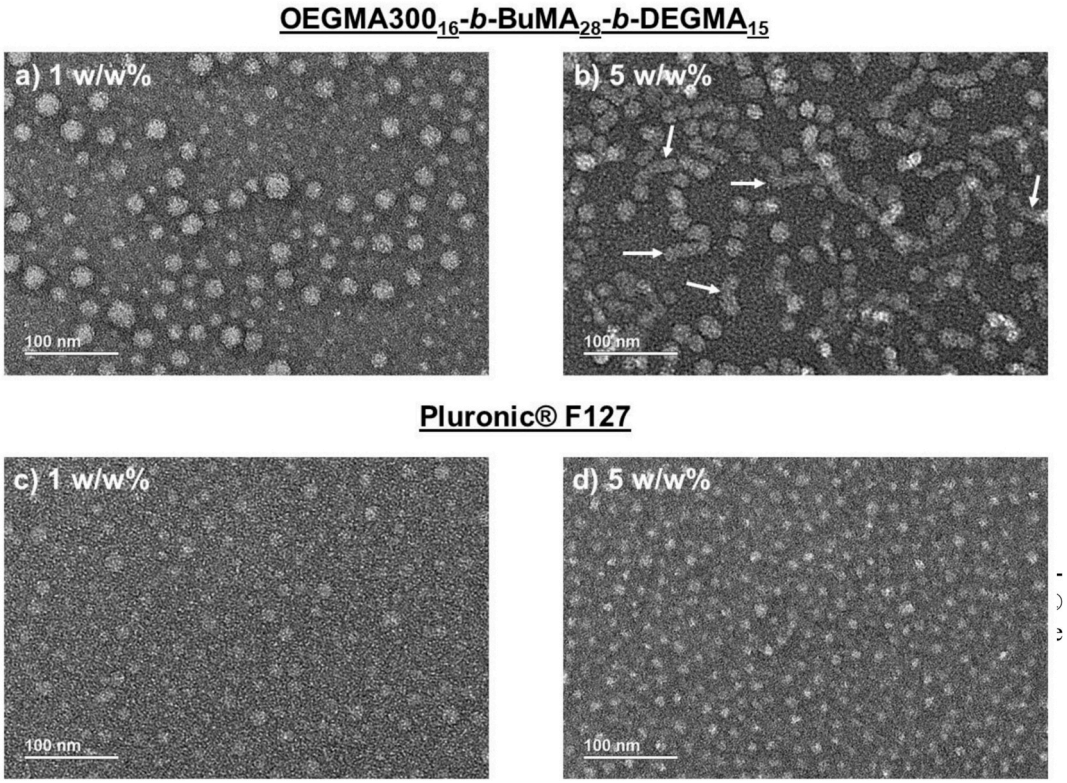

Fig. 3. Transmission Electron Microscopy (TEM) images of: Top – sample of OEGMA300$_{16}$-*b*-BuMA$_{28}$-*b*-DEGMA$_{15}$ at a) 1 w/w% and b) 5 w/w% in deionised water. Bottom – sample of Pluronic® F127 at a) 1 w/w% and b) 5 w/w% in deionised water. The arrows indicate selected cases of worm-like micelles.

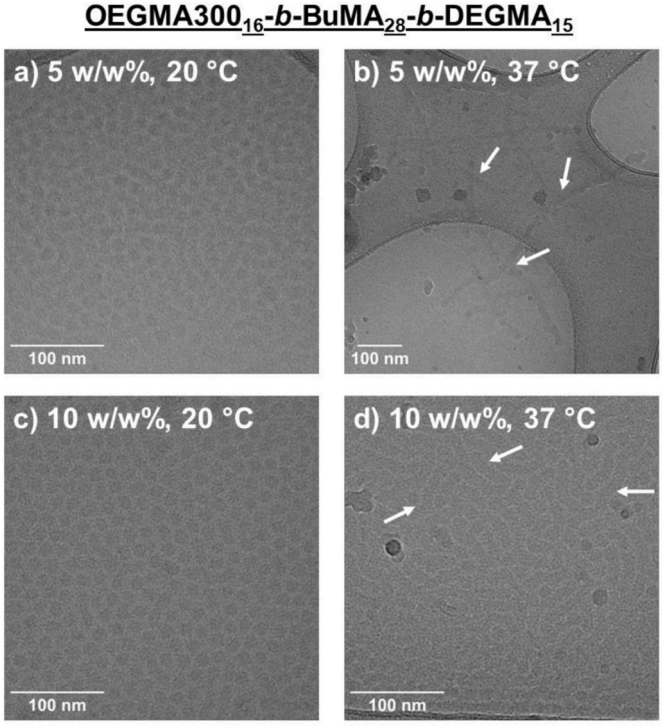

Fig. 4. Cryogenic Transmission Electron Microscopy (Cryo-TEM) images of the OEGMA300$_{16}$-*b*-BuMA$_{28}$-*b*-DEGMA$_{15}$ samples in PBS: Top −5 w/w% at a) 20 °C (solution) and b) 37 °C (gel). Bottom – 10 w/w% at c) 20 °C (solution) and d) 37 °C (gel). The arrows indicate selected mess-like and tubular structures.

at 35 °C, which remains stable up to 46 °C. The decrease in the intensity of the negative peak and shift to higher wavelengths upon heating has previously been observed in PEGylated poly(*L*-glutamate) polymers and attributed to the temperature-induced aggregation above the lower critical solution temperature (LCST) [50].

Pluronic F127 solutions at 1 and 5 w/w% showed similar CD spectra with the negative bands attributed to the n−π* and π−π* of the asymmetric carbon in its PG unit, forming the central thermoresponsive block [45–47]. Notably, the Pluronic F127 samples exhibited minimal changes in MRE with increasing temperature, consistent with the previous results. More specifically, Pluronic F127 solutions at the concentrations studied remain transparent runny solutions upon heating, with the self-assembled structures minimally affected by these temperature and concentration changes, as supported by SANS and TEM analysis.

Following this logic, we suggest that the micellar structures of OEGMA300$_{16}$-*b*-BuMA$_{28}$-*b*-DEGMA$_{15}$ are more dynamic in nature compared to Pluronic F127. Accordingly, the distinct structural changes observed with elevated temperature for the OEGMA300$_{16}$-*b*-BuMA$_{28}$-*b*-DEGMA$_{15}$ samples likely reflect the greater conformational fluctuations and mobility of their micelles, ultimately resulting in heat-induced gelation.

3.5. Molecular origin of the self-assembly

Variable-temperature NMR experiments were previously employed to monitor the thermoresponse of polymers in aqueous media [51–58]. In this study, we performed variable-temperature NMR experiments on 10 w/w% solutions in D_2O for both copolymers to probe the molecular origin of the self-assembly. At this concentration, the OEGMA300$_{16}$-*b*-BuMA$_{28}$-*b*-DEGMA$_{15}$ solution forms a stable gel at 32 °C in PBS and 31 °C in D_2O/PBS, while Pluronic samples do not form a gel at this concentration [59].

The ^{1}H NMR spectra of OEGMA300$_{16}$-*b*-BuMA$_{28}$-*b*-DEGMA$_{15}$, Fig. 6 a), reveal a highly dehydrated BuMA-based core of the self-assembled

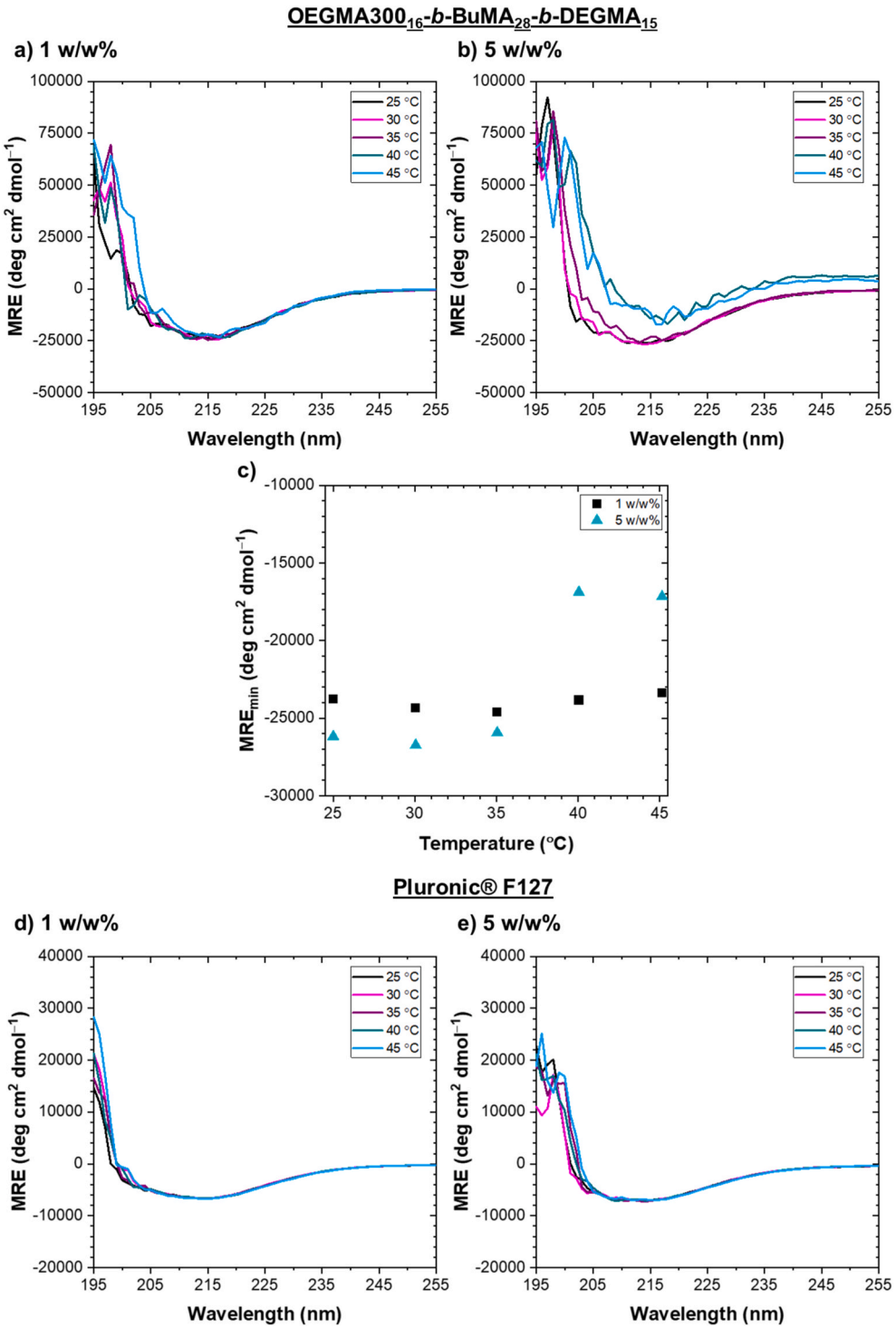

Fig. 5. a) and b) The mean residue ellipticity (MRE) calculated from the temperature variable CD spectroscopy data for OEGMA300$_{16}$-*b*-BuMA$_{28}$-*b*-DEGMA$_{15}$ at 1 and 5 w/w% in PBS, respectively. c) MRE$_{min}$ values as a function of temperature for OEGMA300$_{16}$-*b*-BuMA$_{28}$-*b*-DEGMA$_{15}$ at 1 (black squares) and 5 w/w% (turquoise triangles) in PBS, respectively. d) and e) The MRE calculated from the temperature variable CD spectroscopy data for Pluronic® F127 at 1 and 5 w/w% in PBS, respectively.

structures, as confirmed by the low intensity peaks that correspond to BuMA – see ^{1}H NMR spectrum in $CDCl_3$ (Fig. 6 a)) for comparison. In addition to the low intensity BuMA peaks, the signals corresponding to the backbone protons are also low, indicating minimal interactions of these protons with the solvent. On the other hand, the peaks originating from PEG side chains, which form the corona of the self-assembled structures, are visible in D_2O. While the methoxy peak corresponding to the "e" and "l" protons of OEGMA300 and DEGMA units, respectively, is split in two partially merged peaks in $CDCl_3$, this is not observed in D_2O, presumably due to the DEGMA units also being partially dehydrated at 25 °C, which is close to their cloud point [60]. A decrease in intensity of those peaks is observed as the temperature increases from 25 °C to 31 °C, due to further thermoresponse of the DEGMA units, i.e., transition from a hydrophilic to a hydrophobic state, and consequent formation of a gel. More specifically, the integration of the "d" and "k" protons decreases by 60 %, while the one of the "e" and "l" protons

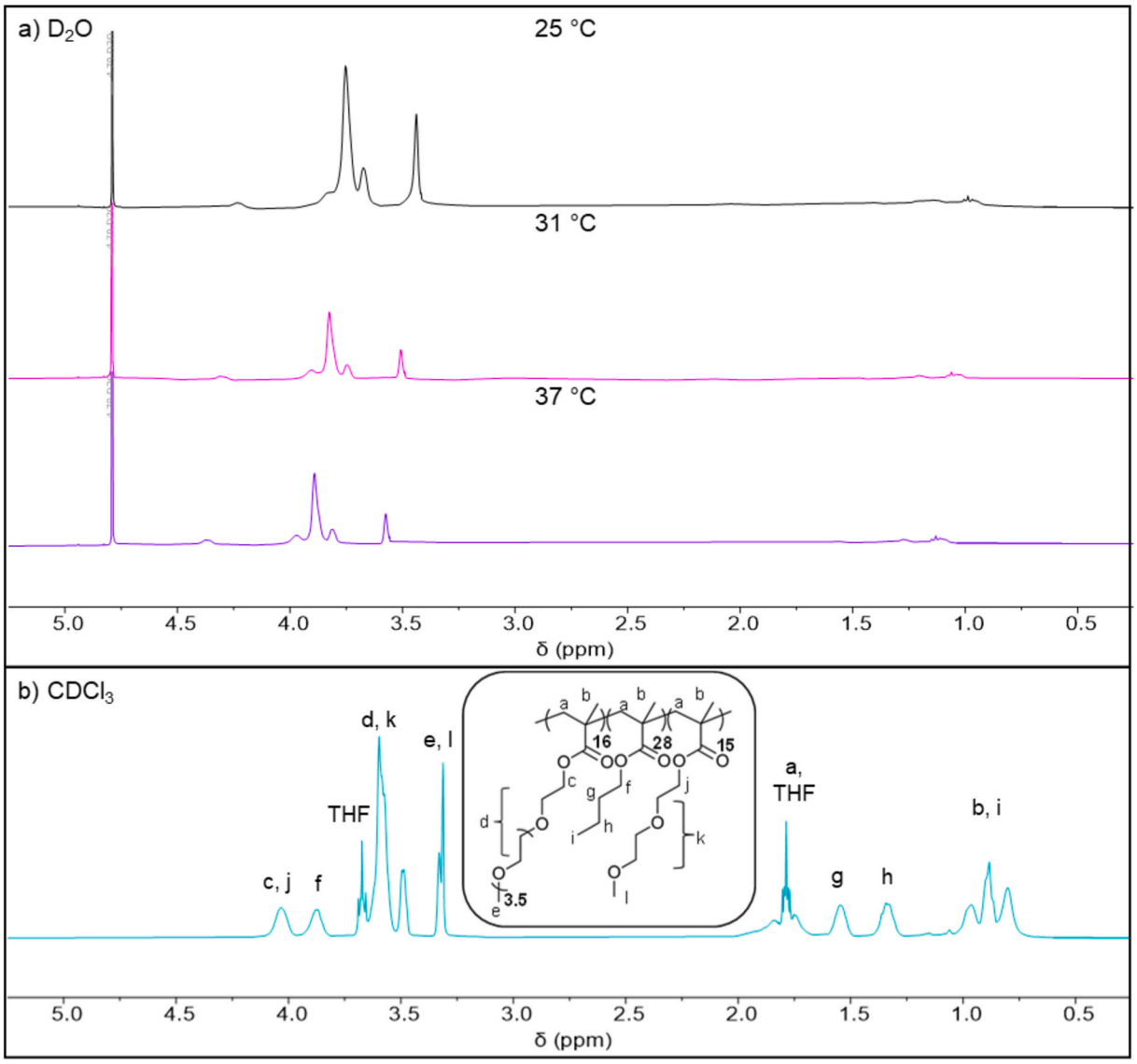

Fig. 6. ^{1}H NMR spectra of OEGMA300$_{16}$-*b*-BuMA$_{28}$-*b*-DEGMA$_{15}$ in D_2O at various temperatures and b) $CDCl_3$ for comparison. The spectra in D_2O were normalised relative to the signal originating from the solvent.

decreases by 80 %, as the temperature shifts from 25 °C to 31 °C. No further decrease is observed when the system is heated further to 37 °C, supporting the visual tests, according to which the sample remains in the gel state. Interestingly, a shift of the peaks to downfield is observed upon heating, which may be attributed to reduced polymer-water hydrogen bonding, as previously observed, and reported [58,61] (See Fig. 7).

Regarding Pluronic F127 samples under the same conditions, the "a" proton of the PEG blocks, and the "b", "c", and "e" protons belonging to the PPG block are visible in both $CDCl_3$ and D_2O, which indicates a greater degree of hydration of these core-forming units when compared to the BuMA ones; note that the "e" protons do not appear in D_2O, due to exchange of the labile -O**H** protons with deuterium in the solvent. No change in the intensity of the peaks is observed upon heating, as expected, due to the sample remaining in solution state at all temperatures tested. However, a shift of the peaks to higher ppm values is observed, similar to the observations made for OEGMA300$_{16}$-*b*-BuMA$_{28}$-*b*-DEGMA$_{15}$, due to reduced polymer-water hydrogen bonding.

4. Conclusions

In this work, we have investigated the self-assembly of diluted solutions of an *in-house* synthesised polymer, namely OEGMA300$_{16}$-*b*-BuMA$_{28}$-*b*-DEGMA$_{15}$, by means of SANS, electron microscopy techniques, CD and NMR spectroscopy experiments at varying temperatures. The self-assembly behaviour was compared directly to Pluronic F127 under the same conditions. In SANS, the effects of temperature and concentration on its self-assembly properties were investigated by testing its aqueous solution at 1 w/w% and 5 w/w% in D_2O/PBS at a range of temperatures. It is noteworthy that at 5 w/w% this polymer solution forms a polymer network, which then destabilises by means of gel syneresis and precipitation. At both concentrations, the resulting SANS patterns were best fitted with an elliptical cylinder model at low temperature, with a significant increase in the length of the cylinder with temperature. More elongated cylinders were formed at 5 w/w%, thus indicating that a polymer network is only formed once a critical length is reached, which sustains the gelation process. The scattering patterns at higher temperatures indicate the presence of scattering inhomogeneities. In contrast, Pluronic F127 forms core-shell spherical micelles, whose core is slightly hydrated at 1 w/w%, while no solvent penetration is observed for the 5 w/w% solution. The self-assembled structures were visualised by TEM, which revealed the presence of tubular/worm-like structures for OEGMA300$_{16}$-*b*-BuMA$_{28}$-*b*-DEGMA$_{15}$,

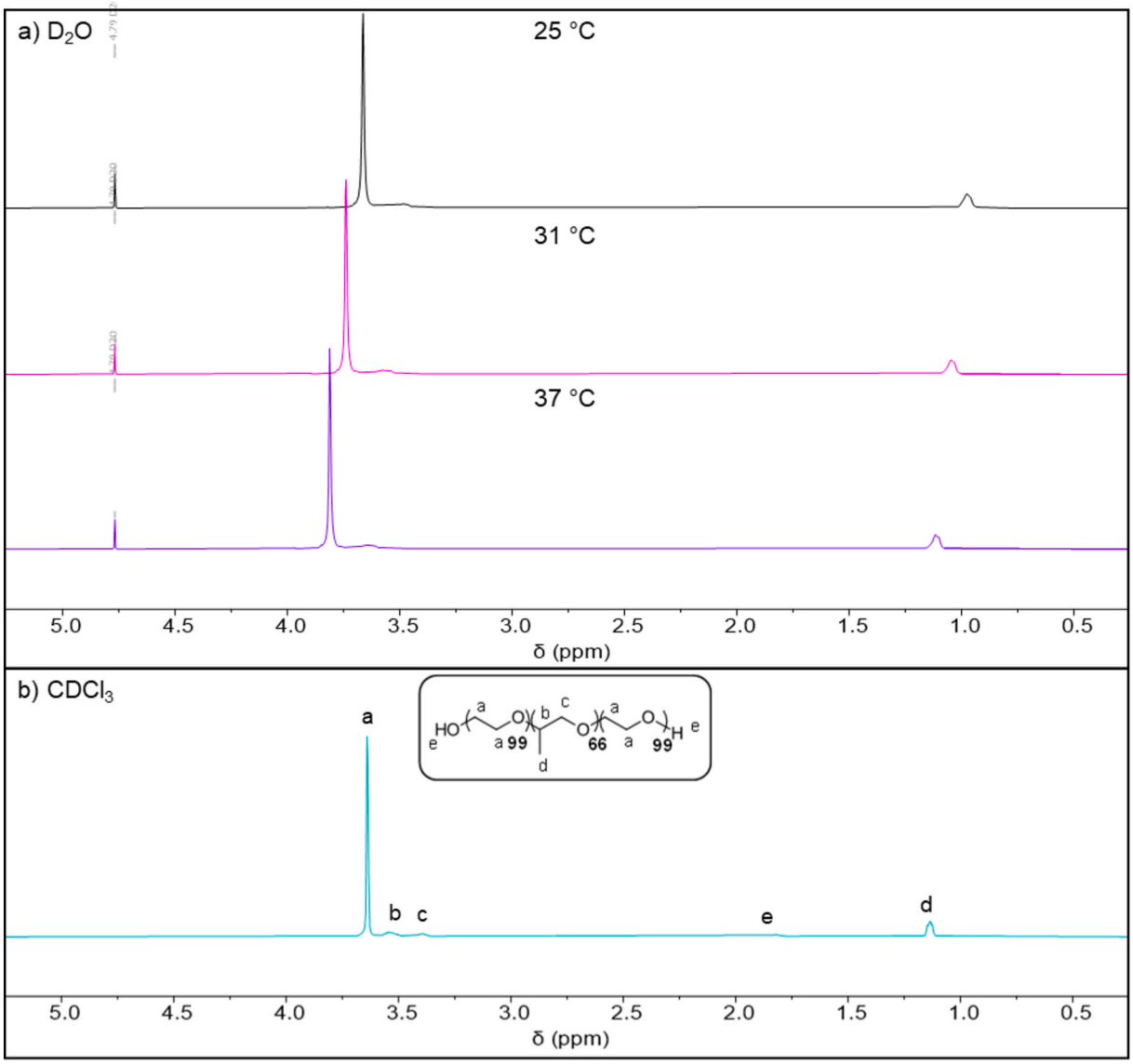

Fig. 7. ^{1}H NMR spectra of Pluronic F127 in a) D_2O at various temperatures and b) $CDCl_3$ for comparison. The spectra in D_2O were normalised relative to the signal originating from the solvent.

while only spherical ensembles were detected for Pluronic F127. Variable-temperature CD and NMR experiments demonstrate the differences between $OEGMA300_{16}$-*b*-$BuMA_{28}$-*b*-$DEGMA_{15}$ and Pluronic F127 and provide complementary information on the molecular origin of the self-assembly. To conclude, this study gives insights on the self-assembly of an ABC triblock terpolymer, which is critical for its low critical gelation concentration.

CRediT authorship contribution statement

Anna P. Constantinou: Writing – original draft, Visualization, Investigation, Formal analysis. **Valeria Nele:** Writing – review & editing, Investigation, Formal analysis. **James J. Doutch:** Investigation, Formal analysis. **Talia A. Shmool:** Writing – review & editing, Investigation, Formal analysis. **Shaobai Wang:** Investigation. **Qian Li:** Investigation. **Jason P. Hallett:** Supervision, Resources. **Cécile A. Dreiss:** Writing – original draft, Formal analysis. **Molly M. Stevens:** Supervision. **Theoni K. Georgiou:** Writing – review & editing, Supervision, Resources, Project administration.

Declaration of competing interest

The authors declare that Prof Georgiou and Dr Constantinou have patented the chemistry of the in house synthesised polymer.

No other financial interests are declared by any of the authors.

Data availability

Data will be made available on request.

Acknowledgments

We gratefully acknowledge Dr Saskia Bakker at the University of Warwick Advanced Bioimaging Research Technology Platform (supported by BBSRC ALERT14 award BB/M01228X/1) for performing the cryo-TEM. A.P.C. acknowledges the Engineering and Physical Sciences Research Council (EPSRC) for the Doctoral Prize Fellowship (EP/M506345/1) as well as the EPSRC Impact Acceleration Grant EP/R511547/1, which has been awarded to TKG's group. V.N. acknowledges the Ermenegildo Zegna Founder's Scholarship program. V.N. and M.M.S. acknowledge funding from the Rosetrees Trust. The SANS

experiments were performed at the ISIS Neutron and Muon Source at the STFC Rutherford Appleton Laboratory, UK, and they were supported by a beamtime allocation from the Science and Technology Facilities Council (1910285). The SANS analysis has been carried out using the SasView software, which was originally developed under the NSF award DMR-0520547. The software contains code the development of which was funded by the European Union's Horizon 2020 research and innovation programme under the SINE2020 project, grant agreement 654000. Mr Bernard Chan is acknowledged for assisting with part of the analysis during his MEng project.

Appendix A. Supplementary data

Supplementary data to this article can be found online at https://doi.org/10.1016/j.polymer.2024.127075.

References

[1] M.T. Cook, P. Haddow, S.B. Kirton, W.J. McAuley, Polymers exhibiting lower critical solution temperatures as a route to thermoreversible gelators for healthcare, Adv. Funct. Mater. 31 (2021) 2008123.
[2] J. Li, et al., Flow induced stability of pluronic hydrogels: injectable and unencapsulated nucleus pulposus replacement, Acta Biomater. 96 (2019) 295–302.
[3] H. Sun, Y. Huang, L. Zhang, B. Li, X. Wang, Co-culture of bone marrow stromal cells and chondrocytes in vivo for the repair of the goat condylar cartilage defects, Exp Ther Med; Experimental and Therapeutic Medicine 16 (2018) 2969–2977.
[4] K. Al Khateb, et al., In situ gelling systems based on Pluronic F127/Pluronic F68 formulations for ocular drug delivery, Int. J. Pharm. 502 (2016) 70–79.
[5] S.H. Lee, J.E. Lee, W.Y. Baek, J.O. Lim, Regional delivery of vancomycin using pluronic F-127 to inhibit methicillin resistant Staphylococcus aureus (MRSA) growth in chronic otitis media in vitro and in vivo, J. Contr. Release 96 (2004) 1–7.
[6] H. Hu, et al., A novel localized co-delivery system with lapatinib microparticles and paclitaxel nanoparticles in a peritumorally injectable in situ hydrogel, J. Contr. Release 220 (2015) 189–200.
[7] M. Müller, J. Au - Becher, M. Au - Schnabelrauch, M. Au - Zenobi-Wong, Printing thermoresponsive reverse molds for the creation of patterned two-component hydrogels for 3D cell culture, JoVE (2013) e50632.
[8] D.B. Kolesky, et al., 3D bioprinting of vascularized, heterogeneous cell-laden tissue constructs, Adv. Mater. 26 (2014) 3124–3130.
[9] R.E. Fitzsimmons, et al., Generating vascular channels within hydrogel constructs using an economical open-source 3D bioprinter and thermoreversible gels, Bioprinting 9 (2018) 7–18.
[10] S. Gardener, G.J. Jones, A new solidifying agent for culture media which liquefies on cooling, Microbiology 130 (1984) 731–733.
[11] S.M. Ng, S. Wieckowski, Stable Hydrogen Peroxide Dental Gel, 4, 1989, p. 156, 839.
[12] C.A. Dreiss, E. Nwabunwanne, R. Liu, N.J. Brooks, Assembling and de-assembling micelles: competitive interactions of cyclodextrins and drugs with Pluronics, Soft Matter 5 (2009) 1888–1896.
[13] I. Grillo, I. Morfin, S. Prévost, Structural characterization of pluronic micelles swollen with perfume molecules, Langmuir 34 (2018) 13395–13408.
[14] M. Valero, W. Hu, J.E. Houston, C.A. Dreiss, Solubilisation of salicylate in F127 micelles: effect of pH and temperature on morphology and interactions with cyclodextrin, J. Mol. Liq. 322 (2021) 114892.
[15] M. Valero, et al., Competitive and synergistic interactions between polymer micelles, drugs, and cyclodextrins: the importance of drug solubilization locus, Langmuir 32 (2016) 13174–13186.
[16] K. Mortensen, W. Brown, B. Nordén, Inverse melting transition and evidence of three-dimensional cubatic structure in a block-copolymer micellar system, Phys. Rev. Lett. 68 (1992) 2340–2343.
[17] V. Castelletto, I.W. Hamley, X.-. Yuan, A. Kelarakis, C. Booth, Structure and rheology of aqueous micellar solutions and gels formed from an associative poly (oxybutylene)–poly(oxyethylene)–poly(oxybutylene) triblock copolymer, Soft Matter 1 (2005) 138–145.
[18] S.J. Byard, et al., Unique aqueous self-assembly behavior of a thermoresponsive diblock copolymer, Chem. Sci. 11 (2020) 396–402.
[19] A. Blanazs, et al., Sterilizable gels from thermoresponsive block copolymer worms, J. Am. Chem. Soc. 134 (2012) 9741–9748.
[20] D.L. Beattie, O.O. Mykhaylyk, A.J. Ryan, S.P. Armes, Rational synthesis of novel biocompatible thermoresponsive block copolymer worm gels, Soft Matter 17 (2021) 5602–5612.
[21] C.C. Hall, C. Zhou, S.P.O. Danielsen, T.P. Lodge, Formation of multicompartment ion gels by stepwise self-assembly of a thermoresponsive ABC triblock terpolymer in an ionic liquid, Macromolecules 49 (2016) 2298–2306.
[22] C. Zhou, G.E.S. Toombes, M.J. Wasbrough, M.A. Hillmyer, T.P. Lodge, Structure of two-compartment hydrogels from thermoresponsive ABC triblock terpolymers, Macromolecules 48 (2015) 5934–5943.
[23] R.R. Taribagil, M.A. Hillmyer, T.P. Lodge, Hydrogels from ABA and ABC triblock polymers, Macromolecules 43 (2010) 5396–5404.
[24] M. Karg, S. Reinicke, A. Lapp, T. Hellweg, H. Schmalz, Temperature-dependent gelation behaviour of double responsive P2VP-b-PEO-b-P(GME-co-EGE) triblock terpolymers: a SANS study, Macromol. Symp. 306–307 (2011) 77–88.
[25] S. Reinicke, et al., Smart hydrogels based on double responsive triblock terpolymers, Soft Matter 5 (2009) 2648–2657.
[26] N. Willet, et al., Fast multiresponsive micellar gels from a smart ABC triblock copolymer, Angew. Chem. Int. Ed. 46 (2007) 7988–7992.
[27] A.P. Constantinou, B. Zhan, T.K. Georgiou, Tuning the gelation of thermoresponsive gels based on triblock terpolymers, Macromolecules 54 (2021) 1943–1960.
[28] O. Arnold, et al., Mantid—Data Analysis and Visualization Package for Neutron Scattering and μ SR Experiments, 764, 2014, pp. 156–166.
[29] Utk, UMD, Nist, ORNL, Isis, ESS, ILL, ANSTO, TU delft, DLS. SasView. 5.0..
[30] R. Serra-Gómez, C.A. Dreiss, J. González-Benito, G. González-Gaitano, Structure and rheology of poloxamine T1107 and its nanocomposite hydrogels with cyclodextrin-modified barium titanate nanoparticles, Langmuir 32 (2016) 6398–6408.
[31] G. González-Gaitano, M.A. da Silva, A. Radulescu, C.A. Dreiss, Selective tuning of the self-assembly and gelation of a hydrophilic poloxamine by cyclodextrins, Langmuir 31 (2015) 5645–5655.
[32] G. González-Gaitano, C. Müller, A. Radulescu, C.A. Dreiss, Modulating the self-assembly of amphiphilic X-shaped block copolymers with cyclodextrins: structure and mechanisms, Langmuir 31 (2015) 4096–4105.
[33] T.A. Shmool, et al., An experimental approach probing the conformational transitions and energy landscape of antibodies: a glimmer of hope for reviving lost therapeutic candidates using ionic liquid, Chem. Sci. 12 (2021) 9528–9545.
[34] M. Kunitz, Syneresis and swelling of gelatin, J. Gen. Physiol. 12 (1928) 289–312.
[35] H.J.M. Van Dijk, P. Walstra, J. Schenk, Theoretical and Experimental Study of One-Dimensional Syneresis of a Protein Gel, 28, 1984, pp. B43–B50.
[36] ftp.ncnr.nist.Gov ⟩ Kline..
[37] A.P. Constantinou, T.K. Georgiou, Pre-clinical and clinical applications of thermoreversible hydrogels in biomedical engineering: a review, Polym. Int. 70 (2021) 1433–1448.
[38] W. Brown, Diffusion of poly(ethylene oxide) in semidilute aqueous solution: dynamic light scattering and gradient diffusion, Polymer 26 (1985) 1647–1650.
[39] W.F. Polik, W. Burchard, Static light scattering from aqueous poly(ethylene oxide) solutions in the temperature range 20-90°C, Macromolecules 16 (1983) 978–982.
[40] A.P. Constantinou, H. Zhao, C.M. McGilvery, A.E. Porter, T.K. Georgiou, A comprehensive systematic study on thermoresponsive gels: beyond the common architectures of linear terpolymers, Polymers 9 (2017) 31.
[41] C. Wu, A. Ying, S. Ren, Fabrication of polymeric micelles with core-shell-corona structure for applications in controlled drug release, Colloid Polym. Sci. 291 (2013) 827–834.
[42] T. Nakano, A. Pietropaolo, M. Kamata, Chirality Analysis of Helical Polymers, 3, 2021, pp. 131–140.
[43] S. Allenmark, Induced Circular Dichroism by Chiral Molecular Interaction, 15, 2003, pp. 409–422.
[44] F. Lebon, et al., Detection by Circular Dichroism of Conformational Transitions in pH and Thermosensitive Copolymers Based on N-Isopropylacrylamide and N-Methacryloyl-L-Leucine, 15, 2003, pp. 251–255.
[45] A. Rodger, P.M. Rodger, Circular dichroism of the carbonyl n-.pi.* transition: an independent systems/perturbation approach, J. Am. Chem. Soc. 110 (1988) 2361–2368.
[46] A. Rodger, M.G. Moloney, n–π* Circular dichroism of planar zig-zag carbonyl compounds, J.Chem.Soc., Perkin Trans. 2 (1991) 919–925.
[47] N. Yoshida, H. Yamaguchi, T. Iwao, M. Higashi, Induced circular dichroism spectra of α-, β-, and γ-cyclodextrin complexes with π-conjugate compounds. Part 2. Chiral dimer formation and polarization directions of the π–π* transitions in some hydroxyazo guests having a naphthalene nucleus, J. Chem. Soc., Perkin Trans. 2 (1999) 379–386.
[48] J. Rao, Z. Luo, Z. Ge, H. Liu, S. Liu, "Schizophrenic" Micellization Associated with Coil-To-Helix Transitions Based on Polypeptide Hybrid Double Hydrophilic Rod–Coil Diblock Copolymer, 8, 2007, pp. 3871–3878.
[49] Y. Tang, L. Liu, J. Wu, J. Duan, Synthesis and self-assembly of thermo/pH-responsive double hydrophilic brush–coil copolymer with poly(l-glutamic acid) side chains, J. Colloid Interface Sci. 397 (2013) 24–31.
[50] C. Chen, Z. Wang, Z. Li, Thermoresponsive Polypeptides from Pegylated Poly-L-Glutamates, 12, 2011, pp. 2859–2863.
[51] M. Vamvakaki, N.C. Billingham, S.P. Armes, Synthesis of Controlled Structure Water-Soluble Diblock Copolymers via Oxyanionic Polymerization, 32, 1999, pp. 2088–2090.
[52] H. Kouřilová, J. Šťastná, L. Hanyková, Z. Sedláková, J. Spěváček, 1H NMR Study of Temperature-Induced Phase Separation in Solutions of poly(N-Isopropylmethacrylamide-Co-Acrylamide) Copolymers, 46, 2010, pp. 1299–1306.
[53] J. Spěváček, NMR Investigations of Phase Transition in Aqueous Polymer Solutions and Gels, 14, 2009, pp. 184–191.
[54] M. Radecki, J. Spěváček, A. Zhigunov, Z. Sedláková, L. Hanyková, Temperature-induced Phase Transition in Hydrogels of Interpenetrating Networks of poly(N-Isopropylacrylamide) and Polyacrylamide, 68, 2015, pp. 68–79.
[55] A. Blanazs, et al., Sterilizable gels from thermoresponsive block copolymer worms, J. Am. Chem. Soc. 134 (2012) 9741–9748.
[56] S.K. Filippov, et al., Internal nanoparticle structure of temperature-responsive self-assembled PNIPAM-b-PEG-b-PNIPAM triblock copolymers in aqueous solutions: NMR, SANS, Light Scattering Studies 32 (2016) 5314–5323.
[57] J. Park, et al., Drug–polymer conjugates with dynamic cloud point temperatures based on poly(2-oxazoline) copolymers, Polym. Chem. 11 (2020) 5191–5199.

[58] H. Fu, et al., Preparation and Tunable Temperature Sensitivity of Biodegradable Polyurethane Nanoassemblies from Diisocyanate and Poly(ethylene Glycol), 7, 2011, pp. 3546–3552.
[59] A.P. Constantinou, et al., Investigation of the Thermogelation of a Promising Biocompatible ABC Triblock Terpolymer and its Comparison with Pluronic F127, 55, 2022, pp. 1783–1799.
[60] Q. Li, A.P. Constantinou, T.K. Georgiou, A library of thermoresponsive PEG-based methacrylate homopolymers: how do the molar mass and number of ethylene glycol groups affect the cloud point? J. Polym. Sci. 59 (2021) 230–239.
[61] S. Han, M. Hagiwara, T. Ishizone, Synthesis of Thermally Sensitive Water-Soluble Polymethacrylates by Living Anionic Polymerizations of Oligo(ethylene Glycol) Methyl Ether Methacrylates, 36, 2003, pp. 8312–8319.

Further reading

[1] T. Georgiou, A. Constantinou, Polymers PCT/GB20 19/052686 (2020).